Janos H. Fendler (Ed.)

Nanoparticles and Nanostructured Films

Preparation, Characterization and Applications

WILEY-VCH

Weinheim • New York • Chichester
Brisbane • Singapore • Toronto

Prof. Janos H. Fendler
Center for Advanced Material Processing
Clarkson University
Potsdam, NY 13699
USA

Library of Congress Card No. applied for.

A catalogue record for this book is available from the British Library.

Deutsche Bibliothek Cataloguing-in-Publication Data:

Nanoparticles and nanostructured films: preparation,
characterization and applications / Janos H. Fendler (ed.). - Weinheim;
New York; Chichester; Brisbande; Singapore; Toronto: Wiley-
VCH, 1998
ISBN 3-527-29443-0

Printed on acid-free and chlorine-free paper.

Composition: Asco Trade Typesetting Ltd., Hong Kong.
Printing: betz-druck gmbh, D-64291 Darmstadt.
Bookbinding: Wilhelm Osswald & Co, D-67433 Neustadt.
Printed in the Federal Republic of Germany.

Chapter 14

Charge Transfer at Nanocrystalline Metal Oxide Semiconductor–Solution Interfaces: Mechanistic and Energetic Links between Electrochromic–Battery Interfaces and Photovoltaic–Photocatalytic Interfaces

B. I. Lemon, L. A. Lyon, and J. T. Hupp

14.1 Introduction

Metal oxide semiconductor films and electrodes displaying only short-range atomic order ("nanocrystallinity") have attracted considerable technological attention because of their typically large effective surface areas, their amenability to dye sensitization, their significant nanoporosity and their often superior charge transport and/or charge storage characteristics [1–3]. Semiconducting oxides of this type typically have been further categorized as either electrochromic/battery materials or as photovoltaic/photocatalytic materials. In particular, those electroactive metal oxides which readily act as intercalation hosts serve as the basis for electrochromic and battery materials [4–5]. On the other hand, those materials for which the conduction band edge lies at a position that is favorable energetically for electron acquisition from light-harvesting species (sensitizing dyes) are candidates for usage in visible-region photovoltaic schemes and UV-region photocatalytic schemes [6–7]. The two types of materials can be prepared by similar methods and in many of the same morphological forms (see description in text). However, as discussed below, widely differing limiting descriptions – based on largely independent historical models – have usually been used to characterize the responses of the two groups of materials to electrochemical and/or photoelectrochemical addition of electronic charge.

For V_2O_5, MoO_3, WO_3 and related materials, electron addition and the attainment of significant dark conductivity is generally accompanied by cation intercalation [8]. As shown specifically in eq. 1 for WO_3, cations are brought into the semiconductor for local charge compensation:

$$W^{VI}O_3 + e^- + M^+ \rightarrow W^{V}O_3(M^+) \qquad (14.1)$$

It is this ability to store cations and thereby stabilize lower metal oxidation states that makes these materials suitable for rechargeable battery applications. When linked to an appropriate counter electrode reaction such as $M^+ + e^- \rightarrow M$, reversal of eq. 1 (i.e. lattice oxidation and cation *de*intercalation) permits electrical energy to be stored.

Often accompanying the electron addition and cation intercalation are changes in the optical absorption spectrum of the material including: a) increases in the apparent optical bandgap (blue shift in the fundamental absorption edge), and b) increases in optical density in the visible and/or near-infrared region [9–10]. Also appearing are dramatic increases in electrical conductivity. While these phenomena clearly are complex, a simplified limiting description emphasizes the role of nominal mixed valency. The availability, at least in a formal sense, of metal centers in multiple oxidation states (V^V/V^{IV}, W^{VI}/W^V, etc.) provides a conceptual basis for electron transport and for intense coloration via long-wavelength light absorption (i.e. optical transitions having intervalence or metal-to-metal charge transfer parentage) [11]. These descriptions can become appreciably altered when account is taken of oxide and/or hydroxide anion mediated metal–metal electronic interactions. The resulting band-type descriptions, however, can still be viewed as descendants of a limiting mixed-valency description.

Wide bandgap materials whose conduction band edges lie at potentials less negative than those of photoexcited dyes are often susceptible to electron injection from surface-bound forms of the dyes (Figure 14.1) and are usually classified as photovoltaic materials. TiO_2, SnO_2, and ZnO are three of the more intensely studied of these semiconductors. Their ability to be prepared in nanocrystalline, high-surface area form allows them to act as particularly efficient light harvesters when employed in dye-sensitized photovoltaic solar cells [1–3]. A typical photovoltaic light-harvesting scheme can be envisaged as shown in Figure 14.1.

Though these semiconductors can be prepared in the same manner as, show similar changes in their optical spectra as, show electrochemistry that can appear identical to, and can exist in similar morphologies as those semiconductors classified as electrochromics, the classical description of how they accommodate excess electronic charge differs dramatically. Indeed, according to the classical model cathodic charging of *n*-type photovoltaic materials results in surface and near-surface electron accumulation (i.e. metal-like behavior) and charge-compensating perturbation of the surrounding electrical double layer (Figure 14.2) [12]. Note that

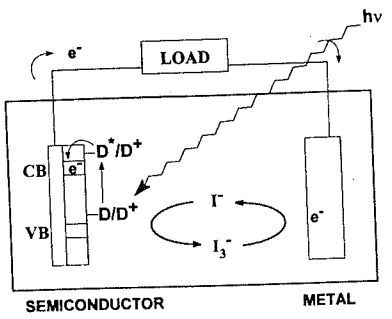

Figure 14.1. A schematic of a dye-sensitized photovoltaic cell. D represents a visible light absorbing dye molecule; D* refers to an electronically excited form of the dye. VB and CB refer to the valence and conduction bands, respectively. I^-/I_3^- is the solution-phase electron "shuttle".

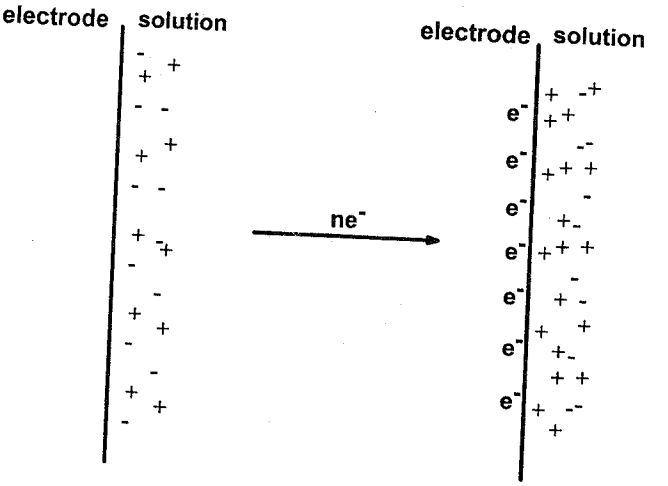

Figure 14.2. Idealized representation of the putative changes in the ionic double layer surrounding a photovoltaic semiconducting electrode under cathodic bias.

in this description, no ion motion *across* the solution/semiconductor interface is necessary for charge compensation.

Recent studies and a careful survey of both bodies of literature, however, lead to new descriptions in which *both* types of materials undergo charge-compensating cation intercalation when subjected to electron addition. In particular, new spectroelectrochemical [13], electrochemical quartz crystal microbalance (EQCM) [14] and photochemical quartz crystal microbalance (PQCM) [15] studies of nanocrystalline semiconductors link the behaviors of the two types of materials under conditions of cathodic charging. As outlined in section *4*, below, these results also lead to a new mechanistic description of the factors controlling the conduction band energetics at the semiconductor/solution interface in nanocrystalline photovoltaic systems. This alternative description could significantly alter the manner in which electrochemical photovoltaic systems are engineered.

14.2 Electrochromics

14.2.1 V_2O_5

Vanandium oxide (primarily V_2O_5) is a layered metal oxide that can be fashioned via a variety of methods including thermal evaporation [16], sputter deposition [17], electrodeposition [18], chemical vapor deposition [19] and sol–gel condensation [20]. For sol–gel produced films, the structure consists of thin "ribbons" connected side-to-side to form layers. Between the layers is interstitial water; these interstitial layers act as cation conduits giving V_2O_5 its excellent intercalation abilities [20]. Though these sol–gel derived films differ morphologically from films prepared via other methods, all films typically display structured, reversible voltammetric responses where the observed peaks are associated with cathodic intercalation and

anodic deintercalation of electrolyte cations [9]. V_2O_5 films offer excellent illustrations of the properties so desired in electrochromic and battery materials. Upon reduction (intercalation) the films show pronounced optical density increases in the visible region [9]. This coloration can be reversible, partially reversible, or irreversible depending on the precise film morphology and the degree of intercalation. Vanadium oxide's ability to store large amounts of cations reversibly (for example, up to 4 Li^+ per formula unit) [21] and to undergo many reversible intercalation/deintercalation cycles [22] (under appropriately controlled conditions) also make it a viable battery material. The details of the intercalation processes have been delineated via various surface analysis, electronic spectroscopy and diffraction investigations, in addition to UV–Vis and cyclic voltammetry studies; the reader is referred to the original literature for further information [8].

14.2.2 MoO_3

MoO_3 is similar to V_2O_5 in many respects. Electroactive films can be prepared by many of the same methods (vacuum and sputter deposition, sol–gel condensation, electrodeposition, anodization, and chemical vapor deposition) [8]. It can exist in either a layered or framework structure; again, the layered structure can intercalate significant quantities of charge- compensating cations [8, 23]. Following V_2O_5, cathodic charging leads to cation intercalation and increases in the visible- region optical absorbance [24] and electrical conductivity [25] of the material. Figure 14.3 shows a voltammetric scan of an electrodeposited MoO_3 film in $LiClO_4$ + propylene carbonate electrolyte solution. A cathodic wave attributed to Li^+ intercalation and an anodic wave representing Li^+ expulsion are noted [24].

MoO_3 is classified as an electrochromic metal oxide due to its reversible and desirable changes in visible-region spectral properties. Figure 14.4 shows the change in the visible absorption spectrum accompanying the above voltammetry. As for V_2O_5, the material becomes highly colored upon reduction and transparent following ion extraction [24], though the changes lie primarily in the visible region. MoO_3's ability to intercalate Li^+ cations also makes it suitable for use in lithium secondary batteries [25].

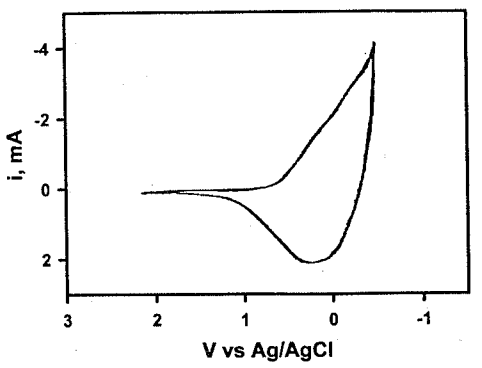

Figure 14.3. Cyclic voltammogram of an electrodeposited MoO_3 film in $LiClO_4$-propylene carbonate. Adapted from ref. 24.

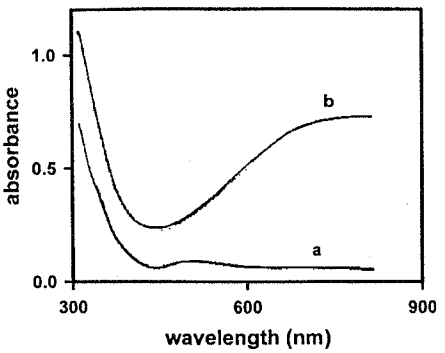

Figure 14.4. UV–Vis spectra of an electrodeposited MoO_3 film at under conditions of: (a) anodic bias and (b) cathodic bias. Adapted from ref. 24.

14.2.3 WO_3

Tungsten oxide makes up the next class of metal oxides used in electrochromics. As for V_2O_5 and MoO_3, WO_3 can be prepared via a wide variety of techniques including chemical vapor deposition [26], rf sputtering [27], sol–gel processing [28], electrochemical deposition [29] and thermal evaporation [30]. WO_3 has been extensively examined as an electrochromic material where the same electron-addition/cation-intercalation/change-in-optical-properties scheme is utilized [8].

Cation intercalation (including H^+, Li^+, and Na^+ intercalation) into WO_3 has been studied in exhaustive detail via methodologies ranging from cyclic voltammetry [31], chronoamperometry [32], impedance spectrometry [32] and electrochemical quartz crystal microgravimetry [29, 32] to EPR [10], Raman [33] and UV–Vis absorption [28] spectroscopies. Figure 14.5 shows a cyclic voltammogram for a sol–gel derived film of WO_3 where the cathodic and anodic waves are attributed to cation intercalation and deintercalation, respectively [10]. Figure 14.6 shows the electro-

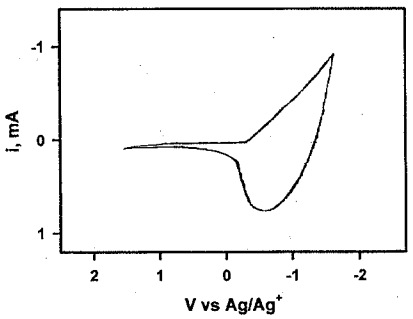

Figure 14.5. Cyclic voltammogram of a sol–gel derived WO_3 film in $LiClO_4$-propylene carbonate. Adapted from ref. 10.

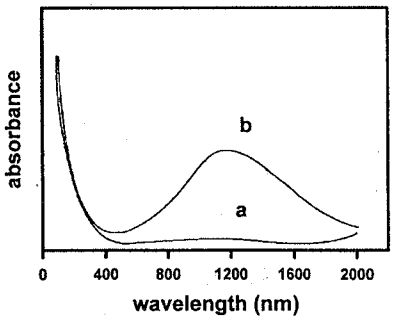

Figure 14.6. UV–Vis spectra of a sol–gel derived WO_3 film in $LiClO_4$-propylene carbonate under conditions of: (a) no external bias, and (b) cathodic bias. Adapted from ref. 10.

chromic behavior of the film. Upon reduction/intercalation, the film becomes intensely colored [10].

More recent reports have employed WO_3 in its high surface area, thin-film form for photochemical applications. Surprisingly, in this form tungsten oxide also shows many of the characteristics of more conventional "photovoltaic" metal oxides. It can, for example, be reduced by UV illumination (and subsequent hole scavenging) either to store electrons for solar energy applications [34] or to react with solution-phase molecules in a photocatalytic scheme similar to that in TiO_2 waste-water remediation [6].

14.3 Photovoltaics

14.3.1 General Observations

In contrast to V_2O_5, MoO_3 and WO_3 which can be reductively doped with protons or alkali metals, the so-called photovoltaic metal oxides are usually assumed to respond to electron addition via electron accumulation layer formation and electrical double layer charging (Figure 14.2, above). Recently, however, Meyer and coworkers have pointed that little, if any, *direct* experimental evidence is available in the extant literature to validate the applicability of the cathodic bias/accumulation layer model to metal oxide systems [35]. These authors instead have pointed to the apparently overwhelming importance of trap states or other localized electronic entities. (In contrast, under conditions of anodic bias, compelling evidence does exist (albeit, for single crystals) for the formation of classical depletion layers [36]).

At the same time, various applications-oriented studies have recently shown that nanocrystalline photovoltaic oxides (most notably, titanium dioxide) can functionally mimic their electrochromic/battery oxide counterparts. In addition, as summarized below, nanocrystalline forms of the *n*-type semiconductors TiO_2, SnO_2 and ZnO have all recently been shown to display (to varying degrees) intercalation behavior during cathodic charging. Observation of these phenomena suggests that ion intercalation may be a *general* mode of reactivity for metal oxide semiconductor/solution interfaces.

14.3.2 TiO_2

The electrochemical addition of electrons to titanium dioxide can be accomplished by scanning the electrode potential or sustaining the electrode bias negative of the apparent conduction band edge. (Except where noted, the form of TiO_2 under discussion in this section is nanocrystalline anatase.) Addition is accompanied by striking increases in conductivity and by conversion of the transparent oxide to a deep blue form [37–38]. It is also accompanied by what is typically termed

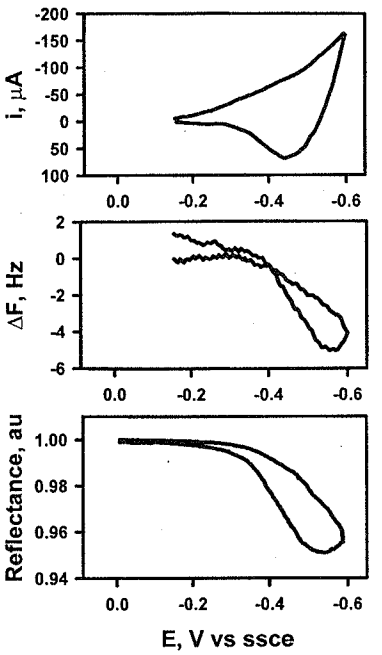

Figure 14.7. EQCM in aqueous media. Panel (a) shows a cyclic voltammogram of a sol–gel derived titanium dioxide film in 1M $HClO_4$. Panel (b) shows reflected laser intensity at 786 nm. Panel (c) shows the change in frequency of the quartz crystal oscillator. Potentials in all three panels are referenced against SSCE.

"capacitive" current flow (cf. Figure 14.2) [39]. Surprisingly, close inspection of the electron addition process via electrochemical quartz crystal microgravimetry (EQCM) has shown that it is appreciably more complex than expected for a purely capacitive process (cf. Figure 14.2), resembling more closely the batterylike process in eq. 1 [14, 40].

EQCM is a valuable analytical tool for the measurement of small mass changes occurring during electrochemical charging of electroactive materials [41]. Application of this technique to high-area titanium dioxide/water interfaces has led to the observation of proton uptake during electron addition. Figure 14.7 illustrates a typical experiment. In panel (a), the addition of electrons is observable by enhanced current flow at potentials negative of the nominal conduction band edge. Simultaneous monitoring of the electrode mass (panel (b)) indicates that the electrode becomes significantly heavier during the apparent charging process. Conclusive evidence for electron addition (as opposed to faradaic current flow) comes from spectroscopic interrogation of the nanocrystalline film. Panel (c) is a laser reflectance spectroelectrochemical scan acquired simultaneously with the data in the preceding panels. The attenuation in the reflected (786 nm) laser intensity is an indication of an increased absorbance due either to conduction band electrons or, more probably, surface trapped or localized electrons (see below). Quantitative analysis of the EQCM data strongly suggests that for each excess electron added, one proton is intercalated into the material. This is further supported by deuterium isotope experiments where the total change in electrode mass doubles upon substitution of H_2O with D_2O as solvent [40].

Proton intercalation has also been reported in a photochemical system [15]. Photoelectrochemical quartz crystal microgravimetry (PQCM) allows for simultaneous monitoring of the electrode mass during bandgap illumination of the semi-

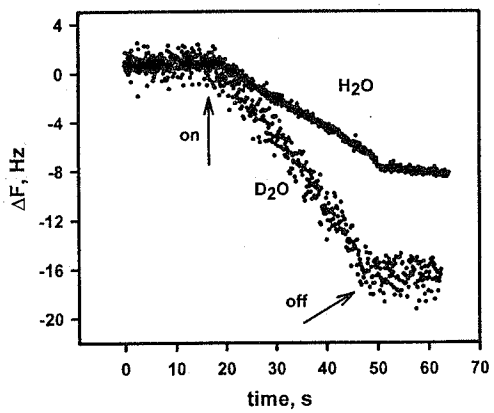

Figure 14.8. PQCM in aqueous media: Change in frequency of the quartz crystal oscillator vs. time for a nanocrystalline titanium dioxide film in contact with H_2O and D_2O. Negative frequency shifts correspond to increases in oscillator mass. Arrows indicate when light is turned on and off.

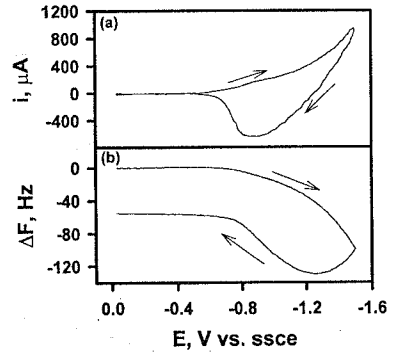

Figure 14.9. EQCM in nonaqueous media: Voltammetry (panel (a)) and microgravimetry (panel (b)) for nanocrystalline titanium dioxide film in scan in acetonitrile containing $LiClO_4$.

conductor. In aqueous media with an appropriate reducing agent (hole scavenger) in solution, proton uptake can be observed as electrons are added to the material. Deuterium isotope experiments showed a mass doubling effect for identical irradiation times (Figure 14.8). These results provide evidence that cation intercalation is necessary for charge compensation, independent of the manner in which electrons are added to TiO_2. Note that evidence (albeit, indirect evidence) for photo intercalation has also been reported for WO_3 [42, 43].

In an early report, Borgarello, et al. described the addition of electrons to colloidal TiO_2 via pulse radiolysis. Subsequent transient conductivity measurements provided evidence for uptake of protons by "reduced" TiO_2 [44].

Perhaps more applicable to the development of charge storage and electrochromic devices are studies of titanium dioxide in nonaqueous media. Of particular interest are voltammetric and EQCM investigations of alkali metal cation intercalation from acetonitrile and propylene carbonate. Grätzel and others have shown via voltammetry and chronoamperometry that nanocrystalline titanium dioxide has some capacity as an intercalation host in both solvents [45–46]. Corroborative of these findings are EQCM measurements performed in nonaqueous media [14, 40]. These again show that cation intercalation accompanies electron addition for the purpose of charge compensation. Figure 14.9 contains representative voltammetric and microgravimetric scans for lithium ion intercalation from acetonitrile. Similar behavior is observed for sodium ion intercalation. The effect is approximately the

same in propylene carbonate where Li^+, Na^+ and K^+ have all been found (by EQCM) to intercalate into nanocrystalline TiO_2 (ca. 5 nm diameter anatase particles in sintered film form). In contrast to the first three alkali metals, larger cations such as tetraalkylammonium species are – for obvious steric reasons – unable to intercalate from either acetonitrile or propylene carbonate. (While the steric argument is compelling for tetralkylammonium ions, it is less compelling for ions such as potassium that are only marginally larger in diameter than the channel widths available in bulk anatase. For nanocrystalline electrode/solution interfaces, account must be taken of possible surface and near surface gelation, as well as lattice distortions introduced by electron addition itself.) For tetraalkylammonium species, failure to intercalate is experimentally evidenced, in part, by decreased electrochemical capacities (smaller voltammetric currents). It is also evidenced by nonstoichiometric electrode mass changes where the nonstoichiometry is attributed to ion binding via surface adsorption rather than lattice intercalation [14, 40].

Alkali metal ion intercalation studies have recently been extended to the fashioning of a "rocking chair" battery based on a nanocrystalline (anatase) titanium dioxide cathode and a lithium anode [47]. In this case, the ability of titanium dioxide to store charge as intercalated lithium ions allows for its use as a battery material. Others have prepared titanium dioxide composites for use as cathode materials [48]. (Here, however, the materials may be microcrystalline rather than nanocrystalline.) Surprisingly, under appropriate high-temperature conditions, storage device construction based on rutile has also proven feasible [49]. Following device discharge, x-ray studies [49] have provided further evidence for lithium intercalation into composite electrodes.

The rapid coloration achievable with TiO_2 films has led to at least one investigation of the intercalation phenomenon in the context of fast switching electrochromics [13]. While the coloration effect is sometimes ascribed to excitation of added conduction band electrons [37], the almost universal observation of finite-wavelength absorption maxima (typically between ca. 800 and 1400 nm) is suggestive instead of excitation of partially localized or trapped electrons. Similarities between absorption spectra for Ti^{III} [50] and partially reduced titanium dioxide (films or colloids) have been noted and the nominally forbidden d–d absorption of Ti^{III} has been suggested as an alternative basis for nanoparticle coloration. In view of the typically strong red and near infrared extinction achievable with reduced titanium dioxide, however, more probable chromophoric sources are electric-dipole-allowed transitions having intervalence parentage (i.e., significant Ti^{III}-$Ti^{IV} \rightarrow Ti^{IV}$-$Ti^{III}$ character).

14.3.3 SnO_2

While there are fewer reports of cation intercalation into nanocrystalline tin oxide, the available results strongly suggest a similar mechanism of charge compensation. EQCM in aqueous electrolyte yields nearly identical results to those observed for TiO_2 [51]. Conclusive evidence of proton intercalation is again offered by deuterium isotope experiments where mass doubling is encountered when D_2O replaces H_2O

as the solvent [51]. Intercalation has not been reported from nonaqeous media but it is anticipated that alkali metal cation intercalation would occur in the absence of proton sources.

14.3.4 ZnO

Much as with tin oxide, the body of work on cation intercalation into zinc oxide is not very large. Weller has shown that up to 6 electrons can be reversibly added to a single 5 nm ZnO particle [52, 53]. Related EQCM measurements from our lab have shown that proton uptake, rather than diffuse double layer charging, provides the necessary charge compensation [51]. The contention that H^+ is the intercalant is again supported by isotope experiments.

One difference between ZnO and most other metal oxides in this discussion is ZnO's lack of strong near-IR absorbance following electron addition [54]. Another difference is its comparative instability with respect to reduction to metallic form [51, 53]. Both observations are likely related to the well known instability of Zn^I. The instability provides an obvious driving force for disproportionation into Zn^{II} and Zn^0 following trapping of excess electronic charge. The instability would also preclude the observation of Zn^{II}/Zn^I-based optical intervalence transitions, leaving only lower extinction conduction-band electrons (delocalized or untrapped electrons) as potential sources for electrochromic coloration.

14.4 Energetic Considerations

14.4.1 Potentials

Proton-intercalation-based electrochromics such as iridium oxide/hydroxide [55] or tungsten bronzes (Eq. 14.1) exhibit color transition potentials (E_{tr}) that are strongly dependent upon solution pH [56]. At 298K the dependence can be expressed as:

$$E_{tr} = E_{tr}(\mathrm{pH}=0) - (0.059\ \mathrm{V})(p/n)(\mathrm{pH}) \tag{14.2}$$

where p is the proton stoichiometry and n is the electron stoichiometry of the electrochromic reaction. Eq. 14.2, of course, follows in an obvious way from a Nernstian thermodynamic characterization of the redox (or redoxlike) behavior of any system involving formation of a protonated product from a reservoir or solution of variable proton activity. For aprotic systems, such as oxide battery electrodes involving M^+ insertion, Eq. 14.2 can be rewritten with pM and an appropriate open circuit potential in place of pH and E_{tr}, respectively.

Curiously, apparent conduction band edge energies (E_{cb}) for n-type photovoltaic oxides also change systematically with pH [37, 39, 54]. For nanocrystalline titanium dioxide, Nernstian behavior is observable over a truly remarkable range – some

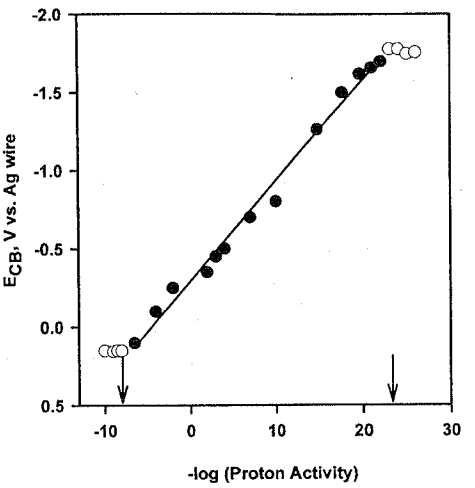

Figure 14.10. Dependence of the conduction band edge energetics (E_{CB}) on proton activity. Arrows at −8 and 24 (open circles) indicate onsets for proton activity independent energy regimes.

32 pH units (Figure 14.10) corresponding to a nearly 2 V variation in E_{cb}! [40] Furthermore, EQCM experiments show that proton intercalation persists at least down to pH = −5 and up to pH = 11. (At more extreme pH's, solution viscosity effects and porous oxide instability effects prevent EQCM interrogation.) Literature explanations for the ubiquitous Nernstian behavior have tended to focus on redox-independent surface protonation effects, i.e. effects responsible for zeta potentials [39]. While perhaps significant over a limited pH range, these explanations are inapplicable at pH's appreciably above the first pK_a or below the last pK_a of the protonated surface oxide. On the other hand, by analogy to eqs. 1 and 3, electron-addition-driven proton intercalation does provide a physical basis for Nernstian changes in photovoltaic metal oxide E_{cb} values over very wide pH ranges. Evidently at $-\log a_{H^+}$ values below −8 and above +24, however, electron addition does ultimately decouple from proton intercalation (see Figure 14.10).

By analogy to battery materials, and in light of recent nonaqueous EQCM findings (Section 2.3), one would also expect (in the absence of proton sources) Nernstian variations in conduction band edge energies with changes in alkali metal ion activity. To the best of our knowledge, experimental studies over an appropriately broad range of activities have not yet been reported. Redmond and Fitzmaurice, however, have described an interesting mixed electrolyte study. They find that lithium perchlorate addition to a dry acetonitrile solution of tetrabutylammonium perchlorate induces large – and apparently non-Nernstian – shifts in E_{cb} for nanocrystalline titanium dioxide [57]. We have observed similar behavior for TiO_2 upon addition of a dry proton source to an aprotic acetonitrile electrolyte solution [14]. While conventional cation adsorption effects presumably contribute in both instances, the predominant energy effect is likely associated with changes in the identity of the cation providing charge compensation.

Closely related are studies of the dependence of energies for electron addition on the cation identity in single electrolyte solutions. Redmond and Fitzmaurice have also demonstrated that titanium dioxide conduction band energies at suitably dried nonhydroxylic solvent interfaces are enormously dependent upon cation size, with larger cations yielding more negative apparent conduction band edge potentials

[57]. These important findings have also been corroborated via EQCM measurements. For the first three alkali metals, the observed energy variations apparently are associated with the increasing difficulty of intercalation, although a role for adsorption effects has also been suggested [14].

Finally, Fitzmaurice and coworkers have also described a remarkable correlation between E_{cb} (TiO_2) and the log of the autoprotolysis constant of the solvent [58]. One possible interpretation is that band edge energetics again are governed by proton intercalation and that solvent variations provide yet another method for achieving extensive H^+ activity variations.

14.4.2 Reactivity Implications

Control of photovoltaic/photocatalytic metal oxide semiconductor interface energetics by intercalation-coupled electron addition has a number of interesting reactivity implications. First, kinetic *de*coupling of electron and cation addition in dye-sensitization schemes can lead to unusual and unexpected reactivity patterns. For example, the kinetics of back electron transfer from nanocrystalline titanium dioxide to at least some surface-bound dye species are pH independent, despite substantial pH-induced changes in overall reaction driving force [59]. On the other hand, the kinetic decoupling effect is evidently not universal. Most notably, rates for electron transfer from titanium dioxide to diffusing or adsorbed methyl viologen are strongly pH dependent [60].

A second implication, in this case from Figure 14.10, is that electron addition to titanium dioxide (and presumably other metal oxides) has an enormous positive effect upon its ability in a thermodynamic sense to take up cations. If the break points in Figure 14.10 are interpreted as effective lattice pK_a's (*not* surface pK_a's), then the internal affinity of titanium dioxide for protons is apparently enhanced by more than 30 orders of magnitude by electron addition [40]. The enhancement implies that "reduced" TiO_2 is capable of abstracting protons even from exceedingly weak acids. If so, then the effect may well be usefully exploitable in new or existing photocatalytic/photochemical remediation applications.

14.5 Conclusions

The availability of processable and electrochemically addressable nanocrystalline forms of *n*-type photovoltaic metal oxides such as SnO_2, ZnO and TiO_2 has revealed that these materials can function as intercalation hosts under conditions of electron addition. Apart from cation intercalation capacity differences, the nanocrystalline photovoltaic materials appear to behave in much the same fashion as oxides traditionally used for battery and electrochromic applications (e.g. layered metal oxides). Indeed, both lithium intercalation batteries and electrochromic thin films can be fashioned from nanocrystalline TiO_2.

The coupling of electron addition to cation intercalation also has important fundamental energetic consequences. Most importantly, the phenomenon appears to account for the remarkable sensitivity of photovoltaic metal oxide conduction band edge energies to pH, solvent identity and electrolyte cation identity. While the available intercalation studies have focused on nanocrystalline materials, related defect-based or gel-layer-based chemistry may well account for the energetics of nominally single crystalline or macroscopically polycrystalline photovoltaic semiconductor/solution interfaces, especially under conditions of negative bias and so-called accumulation layer formation.

Acknowledgment

We thank the Office of Naval Research for support of our work on nanocrystalline metal oxides.

References

[1] O'Regan, B.; Grätzel, M. *Nature*, **1991**, *353*, 737–740.
[2] Grätzel, M. Coord. *Chem. Rev.*, **1991**, *111*, 167–174.
[3] Hagfeldt, A.; Grätzel, M. *Chem. Rev.*, **1995**, *95*, 49–68.
[4] Meyer, G. J.; Searson, P. C. *Interface*, **1993**, *2*, 23.
[5] Kamat, P. V. *Prog. Inorg. Chem.*, **1997**, *44*, 273–343.
[6] Hoffmann, M. R.; Martin, S. T.; Choi, W.; Bahnemann, D. W. *Chem. Rev.*, **1995**, *95*, 69–96.
[7] Kamat, P. V. *Chem. Rev.*, **1993**, *93*, 267–300.
[8] Granqvist, C. G. *Handbook of Inorganic Electrochromic Materials*, 1st ed., Elsevier, Amsterdam, 1995.
[9] Cogan, S. F.; Nguyen, N. M.; Perrotti, S. J.; Rauh, R. D. *J. Appl. Phys*, **1989**, *66*, 1333–1337.
[10] Chemseddine, A.; Morineau, R.; Livage, *J. Solid State Ionics*, **1983**, *9–10*, 357–361.
[11] Livage, J.; Jolivet, J. P.; Tronc, E. *J. Non-Cryst. Sol.*, **1990**, *121*, 35–39.
[12] Gerischer, H. *Electrochim. Acta.*, **1990**, *35*, 1677–1699.
[13] Hagfeldt, A.; Vlachopoulos, N.; Grätzel, M. *J. Electrochem. Soc.*, **1994**, *141*, L82–L84.
[14] Lyon, L. A.; Hupp, J. T. *J. Phys. Chem.*, **1995**, *99*, 15718–15720.
[15] Lemon, B. I.; Hupp, J. T. *J. Phys. Chem.*, **1996**, *100*, 14578–14580.
[16] Audiere, J. P.; Madi, A.; Grenet, J. C. *J. Mat. Sci.*, **1982**, *17*, 2973–2978.
[17] Rauh, R. D.; Cogan, S. F. *Solid State Ionics*, **1988**, *28–30*, 1707–1714.
[18] Burke, L. D.; O'Sullivan, E. J. M. *J. Electroanal. Chem.*, **1980**, *111*, 383–384.
[19] Szörényi, T.; Bali, K.; Hevesi, I. *J. Non-Cryst. Sol.*, **1980**, *35–36*, 1245–1248.
[20] Livage, J. *Chem. Mater.*, **1991**, *3*, 578–593.
[21] Le, D. B.; Passerini, S.; Tipton, A. L.; Owens, B. B.; Smyrl, W. H. *J. Electrochem Soc.*, **1995**, *142*, L102–L103.
[22] Pereira-Ramos, J. P.; Baddour, R.; Bach, S.; Baffier, N. *Solid State Ionics*, **1992**, *53–56*, 701–709.
[23] Julien, C.; Nazri, G. A.; Guesdon, J. P.; Gorenstein, A.; Khelfa, A.; Hussain, O. M. *Solid State Ionics*, **1994**, *73*, 319–326.

[24] Guerfi, A.; Paynter, R. W.; Dao, L. H. *J. Electrochem. Soc.*, **1995**, *142*, 3457–3464.
[25] Julien, C.; Nazri, G. A. *Solid State Ionics*, **1994**, *68*, 111–116.
[26] Davazoglou, D.; Donnadieu, A. *Thin Solid Films*, **1988**, *164*, 369–374.
[27] Akram, H.; Kitao, M.; Yamada, S. *J. Appl. Phys.*, **1989**, *66*, 4364–4367.
[28] Bedja, I.; Hotchandani, S.; Carpentier, R.; Vinodgopal, K.; Kamat, P. V. *Thin Solid Films*, **1994**, *247*, 195–200.
[29] Córdoba de Torresi, S. I.; Gorenstein, A.; Torresi, R. M.; Vázquez, M. V. *J. Electroanal. Chem.*, **1991**, *318*, 131–144.
[30] Ashrit, P. V.; Bader, G.; Girouard, F. E.; Truong, V. *J. Appl. Phys.*, **1989**, *65*, 1356–1357.
[31] Hotchandani, S.; Bedja, I.; Fessenden, R. W.; Kamat, P. V. *Langmuir* **1994**, *10*, 17–22.
[32] Bohnke, O.; Vuillemin, B.; Gabrielli, C.; Keddam, M.; Perrot, H. *Electrochim. Acta.*, **1995**, *40*, 2765–2773.
[33] Delichere, P.; Falaras, P.; Froment, M.; Hugot-Le Goff, A.; Agius, B. *Thin Solid Films*, **1988**, *161*, 35–46.
[34] Bejda, I.; Hotchandani, S.; Kamat, P. V. *J. Phys. Chem.*, **1993**, *97*, 11064–11070.
[35] Cao, F.; Oskam, G.; Searson, P. C.; Stipkala, J. M.; Heimer, T. A. ; Farzad, F.; Meyer, G. J. *J. Phys. Chem.*, **1995**, *99*, 11974–11980.
[36] Lantz, J. M.; Baba, R.; Corn, R. M. *J. Phys. Chem.*, **1993**, *97*, 7392–7395.
[37] Rothenberger, G.; Fitzmaurice, D.; Gratzel, M. *J. Phys. Chem.*, **1992**, *96*, 5983–5986.
[38] Marguerettaz, X.; Fitzmaurice, D. *J. Am. Chem. Soc.*, **1994**, *116*, 5017–5018.
[39] Finklea, H. O. in *Semiconducting Electrodes* (Ed.: H. O. Finklea), Elsevier, New York, 1988, Chapter 2.
[40] Lyon, L. A. *Electrochemical and Photochemical Studies of Polymer Modified and Semiconductor Electrodes*, Ph.D. Thesis, Northwestern University, 1996.
[41] Buttry, D. A. in *Electroanalytical Chemistry* (Ed.: A. J. Bard), Marcel Dekker Inc., New York, USA, 1991, Chapter 1.
[42] Nagasu, M.; Koshida, N. *J. Appl. Phys.*, **1992**, *71*, 398–402.
[43] Bechinger, C.; Herminghaus, S.; Leiderer, P. *Thin Solid Films*, **1994**, *239*, 156–160.
[44] Borgarello, E.; Pelizzetti, E.; Mulac, W. A.; Meisel, D. *Chem. Soc., Farady Trans.* 1, **1985**, *81*, 143–159.
[45] Kavan, L.; Grätzel, M.; Rathousky, J.; Zukal, A. *J. Electrochem. Soc.*, **1996**, *143*, 394–400.
[46] Kavan, L.; Kratochvilova, K.; Grätzel, M. *J. Electroanal. Chem.*, **1995**, *394*, 93–102.
[47] Huang, S. Y.; Kavan, L.; Exnar, I.; Grätzel, M. *J. Electrochem Soc.*, **1995**, *142*, L142–L144.
[48] Ohzuku, T.; Takehara, Z.; Yoshizawa, S. *Electrochim. Acta.*, **1979**, *24*, 219–222.
[49] Macklin, W. J.; Neat, R. J. *Solid State Ionics*, **1992**, *53–56*, 694–700.
[50] Howe, R. F.; Grätzel, M. *J. Phys. Chem.*, **1985**, *89*, 4495–4499.
[51] Lemon, B. I.; Hupp, J. T. *J. Phys. Chem. B*, **1997**, *101*, 2246–2429.
[52] Weller, H.; Eychmüller, A. *Advances in Photochemistry*, **1995**, *20*, 165–217.
[53] Hoyer, P.; Weller, H. *J. Phys. Chem.*, **1995**, *99*, 14096–14100.
[54] Redmond, G.; O'Keefe, A.; Burgess, C.; MacHale, C.; Fitzmaurice, D. *J. Phys. Chem.*, **1993**, *97*, 11081–11086.
[55] Gottesfeld, S.; McIntyre, J. D. E. *J. Electrochem. Soc.*, **1979**, *126*, 742–750.
[56] Pickup, P. G.; Birss, V. I. *J. Electroanal. Chem.*, **1988**, *240*, 185–199.
[57] Redmond, G.; Fitzmaurice, D. *J. Phys. Chem.*, **1993**, *97*, 1426–1430.
[58] Enright, B.; Redmond, G.; Fitzmaurice, D. *J. Phys. Chem.*, **1994**, *98*, 6195–6200.
[59] Yan, S. G.; Hupp, J. T. *J. Phys. Chem.*, **1996**, *100*, 6867–6870.
[60] Moser, J.; Grätzel, M. *J. Am. Chem. Soc.*, **1983**, *105*, 6547–6555.